Received: 18 November 2024 | Revised: 10 February 2025 | Accepted: 11 February 2025

DOI: 10.1002/pro.70079

RESEARCH ARTICLE

THE PROTEIN SOCIETY WILEY

Comparison of enriched charge variants from different anti-CD3 bispecific antibodies reveals differential susceptibility of each bispecific arm to post-translational modification

Jennifer B. Nguyen[1] | **Sophia Liu**[1] | **Dylan A. Howie**[1] | **Zachary R. Oberholtzer**[1] | **Eric T. Ong**[1] | **Ramya Rao**[1] | **Jethro E. Prinston**[1] | **Igor Dikiy**[1] | **Jikang Wu**[2] | **Zhijie Wu**[2] | **Yimeng Zhao**[2] | **Meinuo Li**[2] | **Rosalynn Molden**[2] | **Guido Molina**[3] | **Kathleen Provoncha**[3] | **Cristinel Sandu**[3] | **Haibo Qiu**[2] | **Ning Li**[2] | **William Matousek**[1] | **Michael P. Rosconi**[1] | **Erica A. Pyles**[1]

[1]Protein Biochemistry, Regeneron Pharmaceuticals, Inc., Tarrytown, New York, USA

[2]Analytical Chemistry, Regeneron Pharmaceuticals, Inc., Tarrytown, New York, USA

[3]Therapeutic Proteins, Regeneron Pharmaceuticals, Inc., Tarrytown, New York, USA

Correspondence
Jennifer B. Nguyen, Protein Biochemistry, Regeneron Pharmaceuticals, Inc., 777 Old Saw Mill River Road, Tarrytown, NY 10591, USA.
Email: jennifer.nguyen@regeneron.com

Review Editor: Aitziber L. Cortajarena

Abstract

Charge heterogeneity is an important quality attribute of therapeutic antibodies, and a detailed understanding of charge heterogeneity arising from post-translational modifications (PTMs) is required by regulatory agencies during drug development. Among antibody therapeutics, the bispecific antibody with two distinct Fab domains targeting distinct antigens provides additional complexity to the charge profile. In this study, charge variant species were enriched from three bispecific antibodies (bsAbs) each containing one anti-CD3 binding arm designed with differential affinity to CD3. The charge heterogeneity corresponding to each anti-CD3 arm within each enriched fraction was evaluated using a domain-specific, digestion-assisted imaged capillary isoelectric focusing (icIEF) method known as DiCE. Through fractionation, we observed that the anti-CD3 arm of each bispecific antibody exhibited different distributions of acidic variants, even when the anti-CD3 arms were identical based on primary sequence. Reduced peptide mapping was performed on specific fractions to identify unique site-specific PTMs that were uncovered or enriched through fractionation. In each case, the bispecific arm that was most susceptible to PTMs exhibited a more basic isoelectric point. Conformational stability analysis of each bispecific antibody using differential scanning calorimetry suggested that the more basic Fab arm tended to be correlated with a lower melting temperature, although it is unclear the extent to which PTMs on the basic arm may contribute to reduced conformational stability. Overall, these results provide additional evidence that each of the two arms of a bispecific antibody may exhibit differential susceptibility to post-translational modification and that this susceptibility is likely correlated with subtle differences in overall bispecific antibody

structure, which is influenced by electrostatic properties inherent to the primary sequence. Future studies to obtain high-resolution structures of full-length bispecific antibodies by crystallography or cryo-electron microscopy may help to elucidate the driving force for susceptibility to PTMs in bispecific antibodies.

KEYWORDS
analytical characterization, bispecific antibodies, CD3, imaged capillary isoelectric focusing, post-translational modification

1 | INTRODUCTION

Bispecific antibodies (bsAbs) have emerged as the next-generation antibody-based therapeutic modality to traditional monospecific monoclonal antibodies (mAbs), with the specific advantage of being designed for dual functionality by targeting two antigens (bispecific) or distinct epitopes on the same antigen (biparatopic) (DaSilva et al. 2020; Frankel and Baeuerle 2013; Gunasekaran et al. 2010; Li et al. 2020; Liu et al. 2015; Niquille et al. 2024; Smith et al. 2015). In oncology, bsAbs have been developed to redirect T cells to tumor cells displaying a specific antigen, which can exert multiple anti-tumor effects or potentiate T-cell activation, leading to increased anti-tumor activity.

Several T-cell engaging antibodies have been developed across the biopharmaceutical industry since the early 1980s (Saini and Kumar 2021; Willems et al. 2005). More recently, bispecific antibodies with one arm targeting a T-cell receptor and one arm targeting a tumor-specific antigen (TSA) have been developed. Within the past 2 years alone, eight new bispecific antibodies have been approved, with hundreds of unique T-cell receptor targeting bispecific antibodies currently in clinical trials at various stages (Klein et al. 2024; Middelburg et al. 2024; Paul et al. 2024; Surowka and Klein 2024; Wei et al. 2022).

Among T-cell receptor targets, the CD3 protein complex and T-cell co-receptor are present on all T cells and have become a highly desirable target for developing immunomodulatory approaches for cancer therapy (Menon et al. 2023). The CD3 protein complex itself contains four distinct subunits, which assemble and function as three pairs of dimers, providing a high degree of modularity and tunability of T-cell activation, which can be further tuned through antibody-based therapeutics targeting different subunits. Despite the myriad advantages, targeting CD3 has been associated with adverse effects, including liver toxicity, cytokine release syndrome (CRS), respiratory failure, and tachycardia (Middelburg et al. 2021). As a result, prudent design of anti-CD3 bsAbs must balance these risks against the desired therapeutic effect by fine-tuning expected binding affinity and potency (Lim 2020).

Even with fine-tuning of the immunomodulatory response, the potency of anti-CD3-containing bsAbs may be affected by post-translational modifications within the anti-CD3 regions. Post-translational modifications are often associated with an increase in charge heterogeneity and can occur during protein expression, manufacturing, or storage. We recently reported an imaged capillary isoelectric focusing (icIEF) method, known as DiCE, for quantitating domain-specific charge variants in bsAbs. In this study, we present a workflow that combines charge variant enrichment via chromatography with domain-specific charge variant analysis and provide results for three bsAbs generated using the star substitution strategy for bsAb heterodimerization (Tustian et al. 2016). This approach allows us to investigate the susceptibility of the anti-CD3 arm to post-translational modifications, which may in turn affect potency.

Acidic variants of each anti-CD3 targeting bsAb were successfully enriched based on intact icIEF and DiCE; some of these acidic fractions were associated with reduced potency. Further investigation determined that these acidic variants were correlated with the enrichment of specific PTMs or sequence variants in the complementarity-determining region (CDR) of either the anti-CD3 or anti-TSA arm. Interestingly, the anti-CD3 arm of each bispecific antibody evaluated in this study exhibited different distributions of acidic variants, even when the anti-CD3 arms were identical based on primary sequence, suggesting that the primary sequence of each Fab was not solely responsible for its vulnerability to modification. Indeed, the bispecific arm carrying a more basic charge was demonstrated to be more susceptible to PTMs. Analysis of the thermal stability of each bispecific antibody arm using differential scanning calorimetry indicated that the more basic arm tended to be correlated with a lower thermal melting temperature (T_m), suggesting that the thermal stability of each Fab may influence its susceptibility to PTMs. Overall, these results provide evidence that each of the two arms of a bispecific antibody may exhibit differential susceptibility to post-translational modification and that this susceptibility is likely correlated with subtle differences in overall bispecific antibody structure, which is mediated by the more basic heavy chain arm.

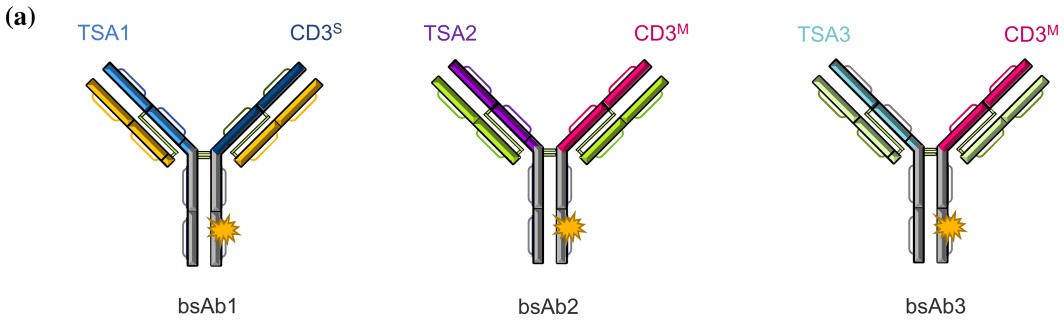

(b)

CD3 Fd	bsAb1	bsAb2	bsAb3
bsAb1	100		
bsAb2	95.8	100	
bsAb3	95.8	100	100

(c)

LC	bsAb1	bsAb2	bsAb3
bsAb1	100		
bsAb2	83.7	100	
bsAb3	84.2	99.1	100

FIGURE 1 (a) Diagrams of the three anti-CD3 bispecific antibodies applied to this study. bsAb1 utilizes a high affinity anti-CD3 arm (Smith et al. 2015) whereas bsAb2 and bsAb3 utilize a moderate affinity anti-CD3 arm. Note that bsAb2 and bsAb3 share the same anti-CD3 monoclonal heavy chain (Fd region denoted in pink) with only minor differences in light chain sequences (green and light green). (b) Sequence similarity within the CD3 Fd domains shared among bsAb1, bsAb2, and bsAb3. (c) Sequence similarity within the LC domains shared among bsAb1, bsAb2, and bsAb3. TSA1, TSA2, and TSA3 refer to three distinct antigens wherein the anti-TSA Fd domains (CDR regions) exhibit no sequence homology.

2 | RESULTS

2.1 | Enrichment of charge variants from three anti-CD3 antibodies

The charge variants of three bsAbs that target separate TSAs with moderate (M) to strong (S) CD3 affinity (Haber et al. 2021) (Figure 1a) were enriched using a combination of molecule-specific, empirically determined ion exchange chromatography steps (Baek et al. 2020; Hirsh and Hirsh 2008; Zhang et al. 2013). Bispecific antibodies bsAb2 and bsAb3 share identical anti-CD3 heavy chain (HC) arms and a highly similar light chain (LC) sequence, which differs by only two amino acid residues. The anti-CD3 arm and LC of bsAb1 share >95% and >84% sequence homology, respectively, with the other two molecules. TSA1, TSA2, and TSA3 refer to three distinct antigens for which the anti-TSA sequences share no appreciable homology within the CDR (Figure 1) (Baek et al. 2020; Hirsh and Hirsh 2008; Zhang et al. 2013).

The fractionation method yielded at least three acidic, one main, and at least one basic fraction for each bsAb molecule. The resultant intact icIEF profiles generated for each enriched fraction (Figure S1, Supporting Information) demonstrate successful enrichment of multiple acidic variants and basic variants to high purity.

2.2 | Domain-specific DiCE analysis of each enriched charge variant sample can provide detailed impurity analysis

The domain-specific charge heterogeneity of each sample was further evaluated using DiCE analysis, in which each sample was pretreated with IdeS enzyme prior to icIEF analysis under reduced, denaturing conditions (Figure 2a–c) (Liu et al. 2024). This methodology provides additional domain-specific charge variant analysis, which can often distinguish modifications on the Fc, LC, and each Fd arm.

2.2.1 | Evaluation of the Fc region of DiCE reveals specific enrichment of PTMs and anti-TSA parental impurities in enriched acidic fractions

For bsAb1, peaks 1–7 (pI ~6.2–6.8) correspond to the Fc/2 or Fc*/2 species generated by sample treatment. More specifically, peaks 2, 4, and 6 correspond to acidic, main, and basic charge variants of the Fc/2 fragment, whereas peaks 3, 5, and 7 correspond to variants of the Fc*/2. Peaks 6 and 7 refer to the unclipped C-terminal lysine of each Fc/2 or Fc*/2 fragment, respectively. Visual inspection of the DiCE profiles

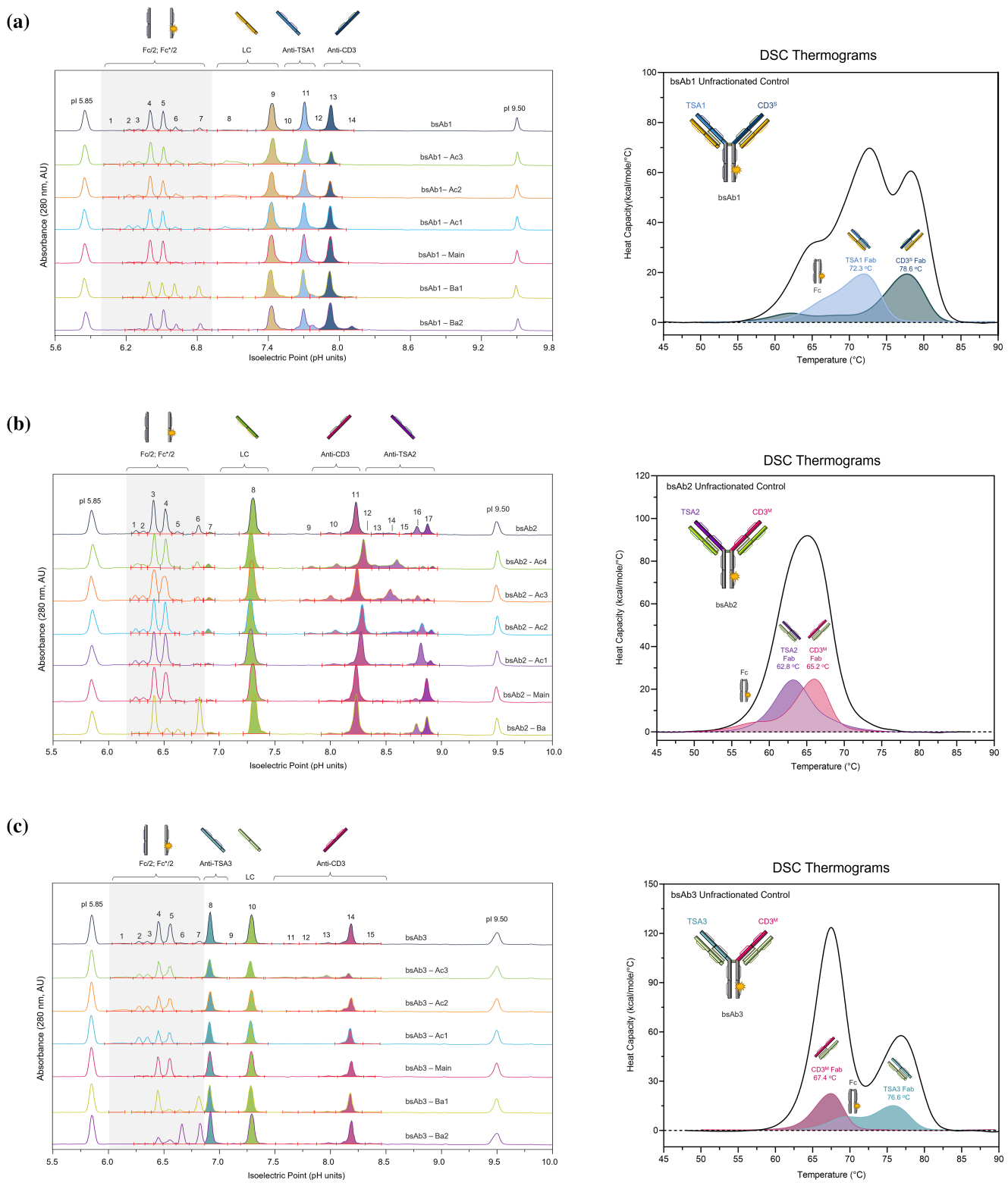

FIGURE 2 Differential susceptibility of bsAb arms to post-translational modification may be influenced by pI and/or thermal stability. (left panels) DiCE analysis of unfractionated and enriched charge variants of (a) bsAb1, (b) bsAb2, and (c) bsAb3. (right panels) DSC thermograms of each bsAb (black solid lines) and its respective parental monospecific mAbs (shaded regions) are also provided for comparison of thermal stability.

generated for the three bsAb sample sets revealed an interesting pattern: if a single C-terminal lysine variant was enriched in a basic fraction, this residue was present on the star (anti-CD3) arm. This result suggests that the C-terminal lysine residue tended to be preferentially hydrolyzed from the non-star (anti-TSA) arm;

however, the mechanism for this chain-specific or sequence-specific susceptibility is unclear.

Additional quantitative analysis of the Fc region of the DiCE profiles from these samples also revealed enrichment of undesirable monospecific parental mAb impurities which may have been carried through the purification process. In this bsAb format, the Fc* domain contains a double substitution (HY → RF) which reduces binding affinity to Protein A compared to the native Fc domain sequence (Tustian et al. 2016). This substitution facilitates effective separation of the desired bsAb product from monospecific parental mAb (Fc/Fc and Fc*/Fc*) byproducts during the affinity capture step of the purification process based on differential affinity to Protein A. Because a completely homogeneous bsAb sample should contain one copy each of the Fc and Fc*, the theoretical ratio (by area) of all Fc peaks relative to all Fc* peaks should be ∼1.0, as observed in the unfractionated and enriched main charge variant samples. However, the area ratio of Fc/Fc* peaks was higher (∼1.47) in acidic variants 1 and 2, suggesting a potential enrichment of the anti-TSA1 monospecific mAb impurity, whereas this ratio was lower (∼0.75) in basic variant 2 (Table S1), suggesting a partial enrichment of the anti-CD3 monospecific mAb impurity in this fraction. No appreciable enrichments of parental impurities were observed for bsAb2 and bsAb3. These results were consistent with quantitation of parental monospecific impurities based on mixed mode (size-exclusion with hydrophobic interaction) chromatography (Table S1) (Zhang and Liu 2016).

2.2.2 | Evaluation of the Fd peaks from enriched charge variant samples reveals a susceptibility to acidic modifications on the Fab arm/Fd fragment exhibiting a more basic pI

With respect to the antigen-binding domains, generally similar levels of peaks corresponding to LC (∼22%–26%) were observed in all enriched fractions corresponding to each antibody. Not surprisingly, enriched acidic fractions tended to exhibit a slightly lower abundance of the predominant LC peak, with a concomitant increase in peaks likely corresponding to an acidic PTM on the LC, which may represent LC glycation or deamidation. In contrast, peaks corresponding to the anti-CD3 or anti-TSA Fd fragments for each of the three bsAb molecules exhibited distinct comparative differences with respect to the number and relative abundance of chain-specific charge variants observed.

In the DiCE electropherogram of bsAb1, two prominent adjacent peaks (peaks 11 and 13) corresponding to the anti-TSA1 and anti-CD3 Fd fragments, respectively, were observed (Figure 2a). These peaks comprise 22.1% and 21.1% of the total peak area, respectively, indicating the expected ∼1:1 molar ratio between the two equivalent Fd arms in the unfractionated bsAb1 product. The enriched acidic 1 (Ac1) and main fractions also exhibited an approximate molar equivalence of these two peaks based on peak area. However, the most acidic charge variants (Ac2 and Ac3) of bsAb1 exhibited a significantly lower abundance of the predominant anti-CD3 peak (9.3%–12.7%) compared to the anti-TSA1 Fd fragment in these fractions (21.3%–24.9%; anti-TSA/anti-CD3 ratio ∼2.0–2.2). This result both suggests a higher abundance of acidic modifications on the anti-CD3 arm and corroborates DiCE observations in the Fc region, which indicated the enrichment of anti-TSA1 parental impurities in these acidic fractions. A significantly higher abundance of the predominant anti-CD3 Fd peak (29.1%) was observed in the most basic fraction (Ba2) of bsAb1, resulting in an anti-TSA/anti-CD3 ratio of ∼0.68, consistent with the Fc/Fc* ratio for bsAb1 (∼0.75) and suggesting enrichment of the anti-CD3 parental monospecific impurity. Two minor basic peaks of the anti-TSA1 and anti-CD3 Fd fragments (peaks 12 and 14) were also observed in the DiCE electropherogram for the most basic fraction; these peaks likely correspond to N-terminal pyroglutamate modifications (data not shown). Although N-terminal pyroglutamate is not expected to impact target binding and potency, this PTM can be sensitively detected using this enrichment workflow.

DiCE analysis of unfractionated bsAb2 revealed three peaks corresponding to the anti-CD3 Fd fragment and five peaks representing charge variants of the anti-TSA2 Fd fragments (Figure 2b), demonstrating that bsAb2 inherently exhibits higher charge heterogeneity than bsAb1. At present, it is unclear whether this charge heterogeneity represents possible differences in downstream bioprocessing or the susceptibility of the molecule itself to post-translational modification during protein expression.

Following charge-based enrichment, acidic fractions Ac4, Ac3, and Ac2 from bsAb2 exhibited a minor increase in the relative abundance of acidic peaks 9 and 10, with a concomitant decrease in the abundance of the main anti-CD3 peak 11 (∼19.1%–19.6%) compared to the unfractionated bsAb2, main, and basic samples (∼22.4-23.3%). These results suggest that only a minor degree of charge variant modifications occurs on the anti-CD3 arm in this molecule. In contrast, the peaks corresponding to the anti-TSA2 Fd exhibited a high level of enrichment of acidic variants, indicating that the surface charge characteristics exploited to enrich the charge variants from bsAb2 were likely dominated by charge heterogeneity occurring on the anti-TSA2 arm.

bsAb2 contains a known CDR glycation on the anti-TSA2 Fd arm (Liu et al. 2024; Xu et al. 2022) which

TABLE 1 Comparison of relative abundance of the predominant Fd or Fd* peaks by DiCE against average relative potency by cell-based bioassay for bsAb1.

	Peak area by DiCE (%)[a]		
bsAb1 sample	**Anti-TSA Fd (%)**	**Anti-CD3 Fd* (%)**	**Average relative potency (%)[b]**
Unfractionated control	22.1	21.1	133 (13)
Acidic 3	21.3	9.3	61 (10)
Acidic 2	24.9	12.7	77 (5)
Acidic 1	22.0	18.5	92 (6)
Main	22.3	21.9	115 (6)
Basic 1	14.8	12.8	80 (15)
Basic 2	19.7	29.1	81 (9)

[a]Values represent the average of triplicate measurements.
[b]Values represent the mean relative potency calculated from three independent determinations. Relative standard deviation is presented in parentheses.

manifests as an acidic variant in DiCE analysis (peak 16) and was specifically enriched in the Ac1 fraction. Additional peaks 12, 13, 14, and 15, corresponding to acidic variants of the anti-TSA2 arm, were enriched in the most acidic fractions. These peaks may include glucuronylation or advanced glycation end products such as carboxymethyllysine as well as oxidation and deamidation PTMs (Wei et al. 2017).

DiCE analysis of bsAb3, which shares an identical anti-CD3 HC and a highly homologous LC sequence with bsAb2 (Figure 1c), revealed three prominent peaks representing the anti-TSA3 Fd (pI ~6.9), LC (pI ~7.2), and anti-CD3 Fd (pI ~8.2) fragments (Figure 2c). Four additional peaks representing anti-CD3 Fd variants were also observed (peaks 11–13). The relative ratio between the most prominent anti-TSA3 Fd peak (peak 8) and the sum of anti-CD3 Fd peaks was approximately ~1.0 for all samples, indicating that even after enrichment, there is low evidence of parental impurity in the unfractionated sample. Interestingly, a significant decrease in the predominant anti-TSA3 Fd fragment was observed in the most acidic fraction (Ac3), along with specific enrichment of acidic peaks 11–13, suggesting that the anti-CD3 Fd sequence used in bsAb2 and bsAb3 is also susceptible to post-translational modification (Table S3).

2.3 | The integrity of the predominant Fd peaks is highly correlated with functional activity

To assess whether the product-related impurities and unique charge variants revealed by this workflow may be correlated with a reduction in functional activity, we evaluated the cell-based potency for each enriched sample using TSA-specific cell-based bioassays and subsequently correlated functional efficacy parameters to key responses determined by the DiCE assay.

Each reporter bioassay was developed to characterize the ability of bsAb1, bsAb2, and bsAb3 to activate TCR/CD3 on reporter cells in the presence of target cells expressing the TSA on the cell surface. This mechanism mimics the process of cell-mediated immunity by redirecting T cells specifically to tumor cells overexpressing TSAs to initiate cell lysis.

For bsAb1, all enriched fractions were functional based on the bioassay, suggesting that any charge variants and/or parental impurities present in each enriched sample were below the (currently undefined) critical threshold required to impact potency (Table 1). In contrast, three of the four enriched acidic variants of bsAb2 exhibited significantly compromised potency (≤50%). Importantly, this reduced potency was consistent with a systematic reduction in the purity of the predominant peak corresponding to the anti-TSA2 Fd based on DiCE analysis (Table 2) and likely correlates with increased abundance of the known CDR glycation modification (Xu et al. 2022). Notably, the main fraction enriched from bsAb2 exhibits no glycation on the TSA2 Fd; this sample was also correlated with a hyperpotent phenotype (>150% potency, relative to the unfractionated reference standard). For bsAb3, only the most acidic enriched variant (Ac3), which exhibited the most unique DiCE profile among all the enriched samples, was correlated with a reduction in cell-based potency (~41%; Table 3). These results demonstrate the capability of DiCE to reveal charge variants and other modifications that have the potential to affect potency.

2.4 | The susceptibility of each bsAb Fab arm to post-translational modification may be correlated with its structural integrity and/or melting temperature

Given that the anti-CD3 Fd arms of bsAb2 and bsAb3 exhibited different levels of post-translational modifications despite sharing an identical primary sequence, we speculated that the differential vulnerability could be related to the solvent accessibility of each Fab arm

TABLE 2 Comparison of relative abundance of the predominant Fd or Fd* peaks by DiCE against average relative potency by cell-based bioassay for bsAb2.

	Peak area by DiCE (%)[a]		
bsAb2 sample	**Anti-TSA Fd (%)**	**Anti-CD3 Fd* (%)**	**Average relative potency (%)[b]**
Unfractionated control	6.0	22.0	71 (6)
Acidic 4	1.1	19.6	14 (13)
Acidic 3	0.9	19.3	22 (22)
Acidic 2	2.2	19.1	41 (32)
Acidic 1	2.1	22.4	66 (4)
Main	11.5	22.5	174 (17)
Basic 1	7.9	23.3	101 (20)

[a]Values represent the average of triplicate measurements.
[b]Values represent the mean relative potency calculated from three independent determinations. Relative standard deviation is presented in parentheses.

TABLE 3 Comparison of relative abundance of the predominant Fd or Fd* peaks by DiCE against average relative potency by cell-based bioassay for bsAb3.

	Peak area by DiCE (%)[a]		
bsAb3 sample	**Anti-TSA Fd (%)**	**Anti-CD3 Fd* (%)**	**Average relative potency (%)[b]**
Unfractionated control	20.9	16.9	97 (4)
Acidic 3	19.7	7.7	41 (2)
Acidic 2	19.9	16.9	84 (4)
Acidic 1	20.5	17.7	95 (3)
Main	22.9	16.0	101 (5)
Basic 1	21.2	17.9	112 (11)
Basic 2	21.6	17.6	90 (1)

[a]Values represent the average of triplicate measurements.
[b]Values represent the mean relative potency calculated from three independent determinations. Relative standard deviation (RSD) is presented in parentheses.

TABLE 4 Comparison of thermal melting temperatures obtained by differential scanning calorimetry (DSC) for the anti-TSA and anti-CD3 Fab arms of bsAb1, bsAb2, and bsAb3.

		T_m (°C)[a]	
Molecule	**Buffer condition**	**Anti-TSA, Fab**	**Anti-CD3, Fab**
bsAb1	10 mM sodium acetate, pH 5.0	72.3 (0.0)	78.6 (0.0)
bsAb2	10 mM acetate, 80 mM NaCl, pH 5.0	62.8 (0.1)	65.2 (0.5)
bsAb3	10 mM histidine, pH 6.0	76.6 (0.0)	67.4 (0.1)

[a]Values represent the average of at least three independent determinations.

within the structure of the intact bsAb. To evaluate this hypothesis, differential scanning calorimetry (DSC) was performed on each bispecific antibody, focusing on the relative melting temperatures (T_m) of each Fab domain (Table 4). In general, the Fab with a lower relative melting temperature and/or onset melting temperature (T_{onset}) suggests lower overall thermal stability (Folch et al. 2010), which may indicate a slightly higher flexibility or solvent accessibility at lower temperatures and allow for enhanced opportunity for non-enzymatic post-translational modifications.

Most monovalent monoclonal antibodies exhibit up to three thermal transitions, correlating to the CH2, CH3, and Fab domains (Ionescu et al. 2008; Ito and Tsumoto 2013). For a bispecific antibody, two separate transitions corresponding to the different Fab domains may be observed. The DSC thermograms for bsAb1 and bsAb3 exhibited multiple thermal transitions, whereas bsAb2 exhibited only a single broad transition (Figure 2). To facilitate data interpretation and confirm peak identities, DSC thermograms for the parental monospecific antibodies were also generated (Figure 2).

We note that DSC buffer systems were specifically optimized for each bsAb (Table 4); however, identical calorimetric enthalpies were observed for the highly

homologous anti-CD3 Fab domains present on bsAb2 and bsAb3 (data not shown), demonstrating comparable intermolecular interactions, including hydrogen bonding, within this domain for both molecules. Furthermore, the observed melting temperature corresponding to the anti-CD3 Fab domain of each bsAb sample remained similar (65.2 and 67.4°C, respectively), despite using different buffer systems, and were identical within the same buffer systems (data not shown). These results further demonstrate adequate robustness within our selected method parameters and support a global comparison among the three bsAb molecules.

Based on our analysis, a general trend relating the T_m of the major Fab transitions and domain-specific charge heterogeneity measured by DiCE analysis appeared evident when comparing across all bsAb molecules. Notably, the Fab arm with the lowest overall T_m (anti-TSA2; 63.0°C) displayed the highest degree of Fd-specific charge heterogeneity among all bsAb samples, whereas Fab arms exhibiting the highest T_m values (anti-CD3 from bsAb1 and anti-TSA3; 78.6 and 76.6°C, respectively) displayed the lowest degree of Fd-specific charge heterogeneity (Figure 2 and Table 4). These results suggest that the differences in apparent PTM susceptibility among each of the Fab arms within the bsAb molecules evaluated in this study may be correlated with their relative conformational stability. Extension of this analysis to additional bsAb and potentially more complex antibody-based products will be critical to evaluating the validity of this proposed hypothesis.

2.5 | Reduced peptide mapping, triggered by DiCE analysis, enables site-specific identification of PTMs that likely correlate with reduced potency

To identify site-specific modifications that may contribute to the formation of charge variants detected by DiCE following enrichment, the unfractionated and enriched samples from all three anti-CD3 bsAbs were subjected to reduced peptide mapping analysis. Sequence identity and site-specific PTMs were characterized using liquid chromatography–tandem mass spectrometry (LC–MS/MS), and extracted ion chromatograms (XIC) were generated to quantify the relative abundance of each PTM.

For bsAb1, a small but steady increase in oxidation and deamidation variants was observed across each enriched acidic variant sample (Table S2). Both oxidation and deamidation PTMs introduce a negative charge at each methionine or asparagine residue, rendering the side chain more polar or acidic. These oxidation and deamidation modifications were generally observed at similar, low levels between the HC (anti-TSA1) and HC* (anti-CD3) arms. The only prominent site-specific PTM observed was the oxidation of an Fc methionine, which was enriched in the Acidic 3 and Acidic 2 fractions (8.3% and 10.5%, respectively). Overall, these results suggest that each arm of bsAb1 may be equally susceptible to oxidation and deamidation.

Peptide mapping results for bsAb2 confirmed the hypothesis that the acidic charge heterogeneity observed within the anti-TSA2 Fd arm was driven primarily by glycation and advanced glycation end products (AGEs) (Fu et al. 1996) located at Lys^{98} (Table S3). Although glycation was the predominant PTM observed in the enriched Acidic 1 fraction for bsAb2, the more acidic fractions were correlated with a higher degree of glucuronylation and carboxymethyl lysine, as well as a +161 Da adduct that is suspected to be another advanced glycation end product.

In the case of bsAb3, the significant reduction of the predominant peak corresponding to the CD3 Fd arm in the Acidic 3 fraction based on DiCE analysis (Figure 2c), correlating with its significantly reduced potency (Table 3), prompted us to investigate the identity and site-specificity of this acidic variant. Although CDR glycation at Lys^{98} on the anti-CD3 Fd might be an obvious possibility based on the experience with bsAb2, no meaningful differences in glycation were observed among the three acidic fractions compared to the unfractionated control sample (5.2%–8.2%; Table S4). Interestingly, an elevated level of Asn deamidation was observed in the bsAb3 Acidic 3 fraction (~3.7%), compared to other acidic fractions and the unfractionated control (~0.1%–0.5%); however, the abundance of this PTM alone was insufficient to account for the >55% decrease in peak area of the predominant anti-CD3 Fd peak observed by DiCE. A closer inspection of the reversed-phase tryptic peptide liquid chromatography chromatograms obtained for the unfractionated control and three acidic fractions revealed a minor but distinct peak that was uniquely observed in the Acidic 3 fraction (Figure 3a). Additional tandem MS/MS experiments indicated that this tryptic peptide corresponded to a novel sequence variant in CDR3 of the anti-CD3 arm of bsAb3, containing two adjacent amino acid substitutions from "LY" to "FF" (Table S4). The identity of this double substitution sequence variant was further validated by comparing the retention time and MS/MS spectra of the peptide observed in the bsAb3 Acidic 3 fraction to that of a synthesized peptide standard containing the same double substitution (Figure 3b,c).

3 | DISCUSSION

Overall, this study presents an effective workflow for assessing potential quality attributes of bispecific antibodies through charge-based enrichment followed by

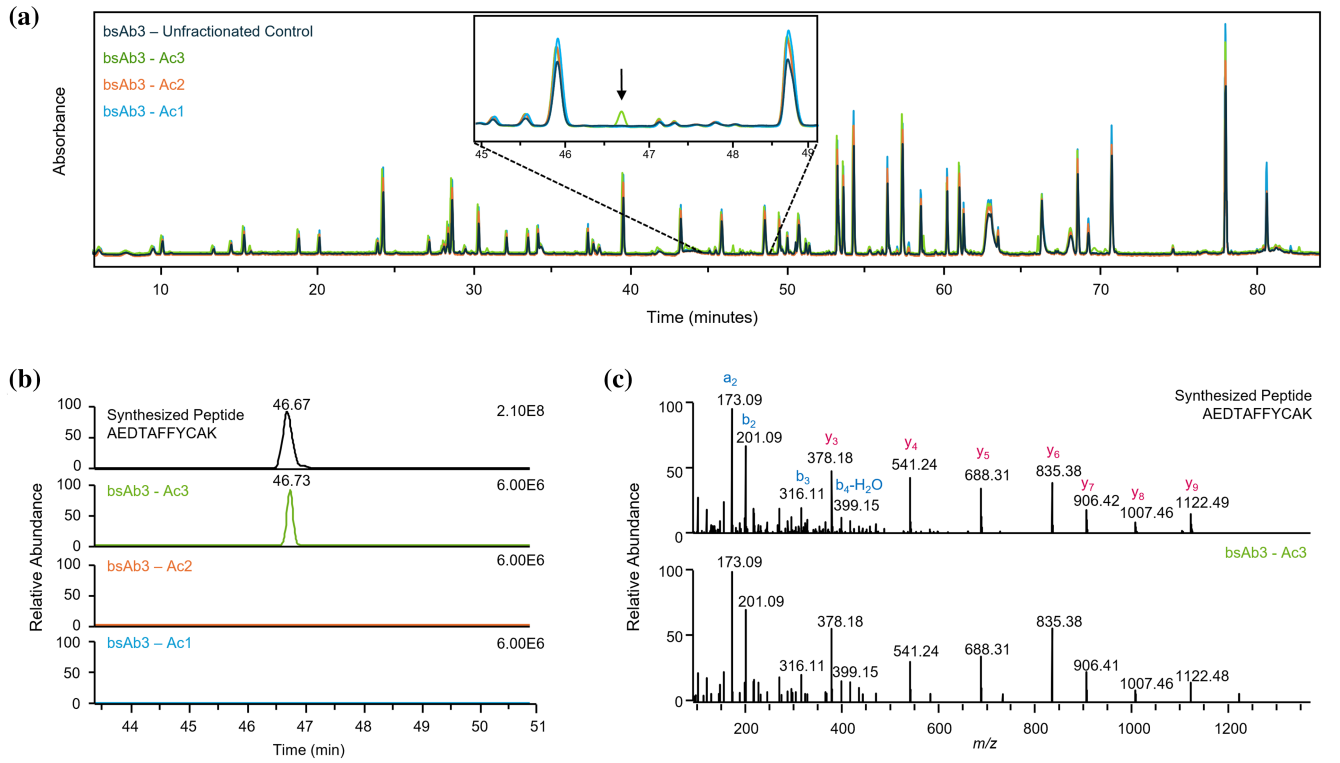

FIGURE 3 Discovery and identification of a novel double substitution sequence variant by peptide mapping. (a) Overlay of reverse-phase UV chromatograms for trypsin-digested bsAb3 unfractionated control, acidic 1, 2, and 3 fractions, including an expanded view to highlight a unique peak of interest appearing at ~46.6 min. (b) Extracted ion chromatograms (XIC) of the *m/z* of a synthetic peptide with amino acid sequence AEDTAFFYC(Carbamidomethyl)AK and the Acidic 1, 2, and 3 fractions from basAb3. (c) MS/MS fragmentation pattern corresponding to the novel peak at ~46.6 min compared against MS/MS results obtained for the synthetic peptide AEDTAFFYC(Carbamidomethyl)AK. The nearly identical XIC elution profile and MS/MS fragmentation pattern confirm the identity of this novel di-amino acid substituted sequence variant.

the evaluation of domain-specific charge heterogeneity and potency. This methodology further validates the utility and versatility of the DiCE assay, presenting a roadmap for in-depth analysis and interpretation of DiCE data, especially in the context of these enriched samples. Not only can DiCE reveal domain-specific charge heterogeneity, but it can provide a qualitative evaluation of parental impurities in partially pure or partially enriched samples. Importantly, the study demonstrated that the integrity of the predominant Fd peak observed in the DiCE electropherogram is highly correlated with functional efficacy, leading to the discovery and identification of a novel double substitution sequence variant in bsAb3.

This double substitution should be considered rare and likely reflects a unique case of natural or environmental selection (Creixell et al. 2012; Gunnarsson and Babu 2023). Indeed, the probability of a spontaneous single nucleotide substitution resulting in a sequence modification is on the order of $\sim 10^{-4}$; the probability of two adjacent random mutations is necessarily even lower ($\sim 10^{-11}$) (Gunnarsson and Babu 2023). Furthermore, leucine and tyrosine are considered slow-evolving amino acids with low relative mutability, further reducing the likelihood of such mutations (Creixell et al. 2012; National Biomedical Research Foundation 1978). Thus, the observed spontaneous mutation from "LY" to "FF" in the CDR3 of the CD3 arm of bsAb3 is highly improbable without environmental influence and/or selective bias, such as an insufficient feed strategy during cell expansion and protein expression. Interestingly, the feed strategy for bsAb3 included an additional tyrosine feed (75 g/L) after inoculation, suggesting sufficient tyrosine levels in the bioreactor. An alternative explanation is that the double substitution variant could have also been contributed by amino acid misincorporation or mischarging by the tRNA during protein synthesis (Raina et al. 2014).

The results from this study also revealed that each bispecific arm may be differentially susceptible to post-translational modification, with the more basic Fab arm tending to be more vulnerable. It could be argued that perhaps the purification processes used during enrichment preferentially select for charge/PTM variants of the more basic Fab arm. However, the three bsAb molecules presented in this case study were enriched using different purification processes: bsAb1 was enriched using a single-step cation exchange process, whereas bsAb2 and bsAb3 were each enriched using a molecule-specific, two-step method combining anion exchange

followed by cation exchange chromatography. Furthermore, each bsAb was formulated at a similar pH and buffer, ensuring a similar chemical environment. Thus, the vulnerability of the basic Fab arm to modifications is more likely due to an inherent feature of the bsAb.

In some ways, the side-by-side comparison of multiple bsAb molecules in this study may have inspired more questions than answers. If the primary sequence dictates the type of PTMs each bsAb will experience, does the absolute pI of each Fab influence susceptibility and/or the distribution of PTMs? Moreover, what is the influence of bsAb structure on susceptibility to PTMs? What is the extent to which PTMs on the basic arm may further contribute to reduced conformational stability?

With respect to the first question, we compared two distinct bsAb (bsAb2 and bsAb3) wherein the anti-TSA arms exhibit dramatically different theoretical and experimental pIs, but the anti-CD3 Fabs were nearly identical. The side-by-side comparison of these molecules by DiCE analysis revealed a similar number of acidic peaks likely correlated with the anti-CD3 arm; however, the distribution of these peaks across the charge-enriched fractions was highly variable. We thus tentatively propose that this anti-CD3 Fab arm may be generally stable to post-translational modifications; however, the juxtaposition of this arm to the anti-TSA arm within the context of the bsAb influences the flexibility of the molecule and therefore its specific distribution of PTMs.

Conformational flexibility between the two Fab arms is an inherent feature of antibodies and is enabled by the IgG hinge motif, generating "Y-shaped," "T-shaped," and "I-shaped" antibodies (Williams et al. 2021). The three bispecific antibodies evaluated in this study contain identical hinge and Fc sequences, so we anticipate that any conformational flexibility would be modulated by the Fab domain. In bispecific antibodies, the tendency toward one particular shape or conformation may be influenced by the surface charge and/or hydrophobicity of each bispecific Fab arm relative to the Fc. This can result in the basic Fab arm becoming more solvent-exposed and thus more susceptible to PTMs.

This emerging hypothesis may be supported by the DSC results. Indeed, the thermal melting temperatures corresponding to the major Fab transitions across all three bsAb molecules generally appear to be correlated with the degree of domain-specific charge heterogeneity observed by our DiCE analysis.

Future studies to evaluate the DiCE profiles and PTMs present within each parental monospecific anti-TSA and anti-CD3 mAb may help to validate this emerging hypothesis. Additionally, obtaining high-resolution structures of full-length bispecific antibodies through crystallography or cryo-electron microscopy may help to elucidate the factors driving their susceptibility to PTMs. Although this study included only three bispecific antibodies, further investigations are already in progress, focusing on other bispecific/biparatopic and alternative format antibodies.

4 | METHODS

All bsAbs used in this experiment were expressed in Chinese hamster ovary cells and produced at Regeneron Pharmaceuticals, Inc. Immunoglobulin G-degrading enzyme of *S. pyogenes* (IdeS) enzyme (FabRICATOR™) was purchased from Genovis, Inc. Urea and guanidine hydrochloride were purchased from Sigma-Aldrich. Carrier ampholytes (pH 5–8 and pH 8–10.5) were purchased from GE Healthcare. The 0.5% methyl cellulose, 1% methyl cellulose, electrolyte solutions (0.08M phosphoric acid in 0.1% methyl cellulose and 0.1M sodium hydroxide in 0.1% methyl cellulose), pI markers 5.85 and 9.50, Transfer Time Measurement (TTM) solution, and fluorocarbon-coated capillary isoelectric focusing (cIEF) cartridges were purchased from Protein Simple, Inc. Bond-Breaker TCEP (tris(2-carboxyethyl)phosphine) solution, 1X Dulbecco's phosphate-buffered saline (DPBS), and Zeba Spin Desalting Plates (7 K molecular weight cutoff) were purchased from Thermo Fisher Scientific. BEH SEC Acquity UPLC Columns (200 Å, 1.7 μm, 4.6 × 300 mm) were purchased from Waters. The remaining chemical reagents were purchased from J.T. Baker.

4.1 | Enrichment technique

Charge variants of bsAb1 were enriched using preparative cation exchange chromatography. Briefly, a Mono S column (10 mm × 100 mm) was pre-equilibrated with 64% mobile phase A (1 mM PiSepB, 2 mM PiSepA, pH 5.0 ± 0.1) and 36% mobile phase B (1 mM PiSepB, pH >10) (Tsonev and Hirsch 2008). bsAb1 was diluted to ~45 mg/mL with 10 mM histidine, pH 5.8, and ~54 mg was loaded onto the column at a flow rate of 5.0–5.5 mL/min. Elution of charge variant forms of bsAb1 was attained by gradually increasing the average ampholyte pI using linear gradients and isocratic hold steps. Fractions were collected in a fraction collector held at 4°C and immediately neutralized with the addition of 200 mM histidine, pH 5.8. Fractions corresponding to each peak were pooled together.

Charge variants of bsAb2 were enriched using two-step preparative ion exchange chromatography. Briefly, a Mono Q column (10 mm × 100 mm) was pre-equilibrated with mobile phase A (40 mM Tris, pH 9.0; 97%) and mobile phase B (45 mM sodium acetate, 100 mM NaCl, pH 5.6). bsAb2 (~50 mg/mL; ~40 mg) was injected onto the column and eluted using a steady gradient of decreasing pH and increasing NaCl, yielding basic and main fractions, as well as a pool of acidic variants. The acidic pool was further separated over a preparative Mono S column (10 mm × 100 mm), pre-

equilibrated in a combination of Mono S buffer A (20 mM MES, pH 5.5; 97%) and Mono S buffer B (40 mM sodium phosphate, 100 mM NaCl, pH 9.0; 3%). Acidic variants of bsAb2 were eluted using a linear gradient of increasing pH and NaCl, resulting in four additional, distinct acidic fractions.

Charge variants of bsAb3 were enriched using two-step preparative anion exchange chromatography. Briefly, a Mono Q column (10 mm × 100 mm) was pre-equilibrated with a combination of 59% mobile phase A (2 mM Tris, 2 mM imidazole, 2 mM piperazine, 16 mM NaCl, pH 4.0 ± 0.1) and 41% mobile phase B (4 mM Tris, 4 mM imidazole, 4 mM piperazine, pH ∼10.5). bsAb3 was diluted to ∼40 mg/mL with 10 mM histidine, pH 6.0, and ∼60 mg was loaded onto the column at a flow rate of 6.0 mL/min. Elution of charge variant forms of bsAb3 was attained by gradually decreasing the average ampholyte pI using linear gradients and isocratic hold steps. Fractions were collected in a fraction collector held at 4°C and immediately neutralized with the addition of 200 mM histidine, pH 6.0. Fractions corresponding to each peak were pooled together.

In addition to the charge variant fractions, unfractionated bsAb1, bsAb2, and bsAb3 controls were analyzed.

4.2 | DiCE analysis

Domain-specific charge heterogeneity of bsAb1 and bsAb2 unfractionated and enriched charge variant samples was evaluated using DiCE following the procedure presented in Liu et al. (Liu et al. 2024).

bsAb3 samples were subjected to identical FabRICATOR digestion conditions as previously reported; however, bsAb3 samples were subsequently diluted to ∼2 mg/mL and exchanged into 1X DPBS supplemented with 5 mM acetic acid and 5 mM Tris (2-carboxylethyl) phosphine (TCEP) for heat denaturation at 80°C for 10 min. Reduced, denatured samples were then neutralized by diluting 2-fold in 8M urea, 120 mM Tris–HCl, pH 7.5, and then buffer exchanged into 35 mM sodium phosphate, 8M urea, and 1 mM TCEP using a Zeba desalting column (0.5 mL, 7 kDa MWCO). The digested samples were then diluted in icIEF sample buffer to produce a final solution containing 21 mM sodium phosphate, 8.3M urea, 0.6 mM TCEP, 0.35% methyl cellulose, 4% (v/v) 3–10 pharmalytes, and 0.5% (w/v) of each pI marker. Data collection and analysis followed the same procedure as previously reported (Liu et al. 2024).

4.3 | Differential scanning calorimetry analysis

Capillary DSC was performed to assess relative thermal stability for each bsAb and its parental mAbs. All experiments were performed in the same manner except that the buffer conditions were optimized for each bsAb (and used for their respective parental mAbs). The sample buffers were 10 mM sodium acetate, pH 5.0; 10 mM sodium acetate, 80 mM NaCl, pH 5.0; and 10 mM histidine, pH 6.0 for bsAb1, bsAb2, and bsAb3, respectively (Table 4). All samples were exchanged into their appropriate sample buffers and subsequently diluted to a concentration of ∼1 mg/mL. The sample buffer was used as the reference buffer. Samples and reference buffer were injected into the Malvern PEAQ-DSC cells in a volume of 325 μL. Briefly, each sample was heated in the sample cell at a scan rate of 90°C/h with the temperature ranging from 15 to 110°C and with a filtering period of 10 s. This was conducted in parallel with the reference cell filled with reference buffer. Differential power was applied to the sample and reference cells to maintain the same heating rate in both cells and was monitored as a function of temperature. Data analysis was performed using MicroCal PEAQ-DSC software. The differential power values (μcal/s) were converted to Cp, (kcal/mole/°C), and each thermogram was background-subtracted and fit with a linear baseline. The total enthalpy of unfolding (ΔH) and thermal melting temperature for each domain was calculated by integration of each thermogram.

4.4 | Bispecific parental impurity analysis by mixed-mode chromatography

bsAb1, bsAb2, and bsAb3 samples were analyzed by mixed-mode chromatography (MMC), combining size-exclusion with hydrophobic interaction chromatography, to quantify peaks corresponding to the respective anti-TSA and anti-CD3 monospecific mAb impurities. Briefly, each bsAb1 sample was buffer exchanged into 1X DPBS and diluted to approximately 5 mg/mL prior to analysis for injection (10–15 μg) at a flow rate of 0.2 mL/min onto a Zenix SEC-300 size-exclusion column (Sepax Technologies; 7.8 mm × 300 mm, 3 μm particle size) pre-equilibrated in 10 mM sodium phosphate, 800 mM sodium chloride, pH 7.0 ± 0.1. The absorbance signal was monitored at 215 and 280 nm, and chromatograms were integrated to determine the relative abundance of each peak. Anti-TSA and anti-CD3 monospecific (parental) mAb samples were prepared separately under the same conditions described above and were included as controls to identify peaks corresponding to each impurity. A similar method was used for bsAb2, except with a flow rate of 0.3 mL/min in the mobile phase containing 20 mM sodium phosphate, 10 mM sodium acetate, 350 mM sodium sulfate, and 160 mM sodium chloride, pH 7.0 ± 0.2. The bsAb3 MMC method was performed at 0.2 mL/min with a mobile phase consisting of 10 mM sodium phosphate, 1.5M sodium chloride, pH 7.0 ± 0.1.

4.5 | Reporter bioassay for TCR/CD3 activation mediated by bsAb1, bsAb2, and bsAb3

Reporter bioassays were developed to characterize the ability of CD3 bsAb1, bsAb2, and bsAb3 to activate TCR/CD3 on reporter cells in the presence of target cells expressing the TSA on the cell surface. Bioassay reporter cells consist of Jurkat cells (immortalized human T-cell lymphocytes expressing TCR/CD3 endogenously) engineered with a luciferase reporter under the control of a NFAT response element. The target cell lines for bsAb1, bsAb2, and bsAb3 consist of individual human cell lines that were selected based on specific TSA expression. The bioassay consists of mixing the reporter cells, target cells, and bsAb and incubating the assay for 4–6 h at 37°C and 5% CO_2. This was followed by the addition of OneGlo™ detection reagent and reading assay plates luminescence in a multimodal plate reader. Each individual bioassay was optimized in terms of reporter: target cell ratio, total cell numbers per well, and bsAb concentration range and dilution factor. The data was analyzed in GraphPad Prism using a four-parameter logistic (4PL) regression analysis without constraints of the raw data with log-transformed concentration values. Each dose–response curve was derived from three intra-plate technical replicates, and each replicate Y-value was considered as an individual point in the 4PL analysis. The reference standard used for each assay was a qualified and representative bsAb lot for each bsAb. The relative potency value for each test article was calculated using Equation (1),

$$\text{Relative potency} = \left(\frac{\text{EC}_{50}\,\text{Reference standard}}{\text{EC}_{50}\,\text{Test article}}\right) \times 100\%. \quad (1)$$

4.6 | Reduced peptide mapping

Peptide mapping analysis for bsAb1 and bsAb2 was performed according to the procedure described in Liu et al. (Liu et al. 2024).

Briefly, bsAb3 was buffer exchanged into 5 mM acetic acid using a Nanosep® 10 K centrifugal filter (Pall Corporation, Port Washington, NY). A 0.1 mg aliquot of the bsAb3 sample was denatured and reduced with 5 mM TCEP-HCl at 80°C for 10 min, diluted with 8M urea, alkylated with 2 mM iodoacetamide, and digested with sequencing grade modified trypsin from Promega (Madison, WI; enzyme-to-substrate ratio of 1:20 w/w) at 37°C in the dark for 3 h. The digested sample was quenched with 5% trifluoracetic acid (TFA).

To validate the identification of the peptide with two adjacent amino acid substitution sites, a synthetic peptide (AEDTAFFYC[Carbamidomethylation]AK, purity >98%, Thermo Fisher Scientific, San Jose, CA) was analyzed on an LC–MS system at a final concentration of 0.1 mg/mL.

LC–MS experiment was performed using an ACQUITY UPLC Peptide BEH C18 column (1.7 μm, 300 Å, 2.1 mm × 150 mm, 1–30 K, Waters Corporation, Milford, MA) on an ACQUITY UPLC I-Class system (Waters Corporation). Mobile phase (MP) Buffer A was 0.05% TFA in Milli-Q water, and Buffer B was prepared with 0.045% TFA in acetonitrile. The gradient was run at 0.25 mL/min, starting with 0.1% MPB from 0 to 5 min, followed by 0.1%–40% MPB from 5 to 90 min, 40%–90% MPB from 90 to 95 min, 90% MPB from 95 to 105 min, 90%–0.1% MPB from 105 to 106 min, and then 0.1% MPB until the end of the 125 min gradient. The column temperature was set to 40°C during the experiment, and 10 μg was injected for each experiment.

The LC system was coupled to a Thermo Scientific Q Exactive Plus Hybrid Quadrupole-Orbitrap mass spectrometer (Bremen, Germany). MS data acquisition was performed through a full scan at a resolution of 70,000 in positive mode with a scan range of 300–2000 *m*/*z*, AGC target at 3e6, and maximum injection time of 100 ms. MS/MS experiments were conducted at a resolution of 17,500, AGC at 1e5, maximum injection time of 100 ms, loop count of 5, and normalized collision energy of 27. The ESI parameters were set with a spray voltage of 3.8 kV, capillary temperature of 320°C, S-lens at 50, sheath gas at 40, auxiliary gas at 10, and auxiliary gas heater temperature of 250°C. Byonic (version 4.6.1, Protein Metrics Inc., Cupertino, CA) was used to perform protein sequence searches and PTM identifications. BioPharma Finder (version 5.0, Thermo Fisher Scientific, San Jose, CA) was utilized for protein sequence searches, PTM identifications, and differential analysis. The relative quantification of PTMs was determined using Skyline-daily software (version 23.1, University of Washington, Seattle, WA). The retention time and MS/MS spectrum match between the identified sequence variant peptide and the synthetic peptide was confirmed using Xcalibur (version 4.1, Thermo Fisher Scientific, San Jose, CA).

AUTHOR CONTRIBUTIONS

Jennifer B. Nguyen: Conceptualization; investigation; writing – original draft; writing – review and editing; formal analysis; supervision; project administration; data curation; methodology; visualization. **Sophia Liu:** Investigation; methodology; conceptualization; formal analysis. **Dylan A. Howie:** Investigation. **Zachary R. Oberholtzer:** Investigation. **Eric T. Ong:** Investigation. **Ramya Rao:** Investigation. **Jethro E. Prinston:** Investigation. **Igor Dikiy:** Investigation; writing – original draft; formal analysis. **Jikang Wu:** Writing – original draft; investigation. **Zhijie Wu:** Investigation; writing – original draft. **Yimeng**

Zhao: Investigation; writing – review and editing. **Meinuo Li:** Investigation. **Rosalynn Molden:** Investigation. **Guido Molina:** Investigation. **Kathleen Provoncha:** Investigation. **Cristinel Sandu:** Investigation; data curation; formal analysis; writing – original draft; writing – review and editing. **Haibo Qiu:** Supervision; writing – review and editing. **Ning Li:** Supervision; writing – review and editing. **William Matousek:** Supervision; writing – review and editing; formal analysis. **Michael P. Rosconi:** Writing – review and editing; supervision; writing – original draft; methodology; data curation; formal analysis. **Erica A. Pyles:** Writing – review and editing; supervision.

ACKNOWLEDGMENTS

The authors gratefully acknowledge Matthew C. Franklin for helpful discussions regarding the conformational diversity of antibody structures, Evan Koufos and Kathir Muthusamy for extending an invitation to investigate charge variants of bsAb3, as well as Lauren Salvador and Raymonda Martin for critical and editorial review of the manuscript.

CONFLICT OF INTEREST STATEMENT

This study was sponsored by Regeneron Pharmaceuticals, Inc. The authors declare the following competing financial interest(s): J.B.N., S.L., D.A.H., Z.R.O., R.R., J.E.P., I.D., J.W., Z.W., Y.Z., M.L., G.M., K.P., C.S., H.Q., N.L., W.M., M.P.R., and E.A.P. are full-time employees and shareholders of Regeneron Pharmaceuticals, Inc. The authors have no other relevant affiliations or financial involvement with any organization or entity with a financial interest in or financial conflict with the subject matter or materials discussed in the manuscript apart from those disclosed.

DATA AVAILABILITY STATEMENT

The data that support the findings of this study are available from the corresponding author upon reasonable request.

ORCID

Jennifer B. Nguyen https://orcid.org/0009-0008-0488-353X

REFERENCES

Baek J, Schwahn AB, Lin S, Pohl CA, Pra MD, Tremintin SM, et al. New insights into the chromatography mechanisms of ion-exchange charge variant analysis: dispelling myths and providing guidance for robust method optimization. Anal Chem. 2020;92(19):13411–9. https://doi.org/10.1021/acs.analchem.0c02775

Creixell P, Schoof EM, Tan CSH, Linding R. Mutational properties of amino acid residues: implications for evolvability of phosphorylatable residues. Philos Trans R Soc Lond B Biol Sci. 2012;367(1602):2584–93. https://doi.org/10.1098/rstb.2012.0076

DaSilva JO, Yang K, Bay AEP, Andreev J, Ngoi P, Pyles E, et al. A biparatopic antibody that modulates MET trafficking exhibits enhanced efficacy compared with parental antibodies in MET-driven tumor models. Clin Cancer Res. 2020;26(6):1408–19. https://doi.org/10.1158/1078-0432.ccr-19-2428

Folch B, Dehouck Y, Rooman M. Thermo- and mesostabilizing protein interactions identified by temperature-dependent statistical potentials. Biophys J. 2010;98(4):667–77. https://doi.org/10.1016/j.bpj.2009.10.050

Frankel SR, Baeuerle PA. Targeting T cells to tumor cells using bispecific antibodies. Curr Opin Chem Biol. 2013;17(3):385–92. https://doi.org/10.1016/j.cbpa.2013.03.029

Fu MX, Requena JR, Jenkins AJ, Lyons TJ, Baynes JW, Thorpe SR. The advanced glycation end product, N^{ϵ}-(carboxymethyl)lysine, is a product of both lipid peroxidation and glycoxidation reactions. J Biol Chem. 1996;271(17):9982–6. https://doi.org/10.1074/jbc.271.17.9982

Gunasekaran K, Pentony M, Shen M, Garrett L, Forte C, Woodward A, et al. Enhancing antibody Fc heterodimer formation through electrostatic steering effects: applications to bispecific molecules and monovalent IgG. J Biol Chem. 2010;285(25):19637–46. https://doi.org/10.1074/jbc.m110.117382

Gunnarsson PA, Babu MM. Predicting evolutionary outcomes through the probability of accessing sequence variants. Sci Adv. 2023;9(30):eade2903. https://doi.org/10.1126/sciadv.ade2903

Haber L, Olson K, Kelly MP, Crawford A, DiLillo DJ, Tavaré R, et al. Generation of T-cell-redirecting bispecific antibodies with differentiated profiles of cytokine release and biodistribution by CD3 affinity tuning. Sci Rep. 2021;11(1):14397. https://doi.org/10.1038/s41598-021-93842-0

Tsonev LI, Hirsh AG. Theory and applications of a novel ion exchange chromatographic technology using controlled pH gradients for separating proteins on anionic and cationic stationary phases. J Chromatogr A. 2008;1200(2):166–82.

Ionescu RM, Vlasak J, Price C, Kirchmeier M. Contribution of variable domains to the stability of humanized IgG1 monoclonal antibodies. J Pharm Sci. 2008;97(4):1414–26. https://doi.org/10.1002/jps.21104

Ito T, Tsumoto K. Effects of subclass change on the structural stability of chimeric, humanized, and human antibodies under thermal stress. Protein Sci. 2013;22(11):1542–51. https://doi.org/10.1002/pro.2340

Klein C, Brinkmann U, Reichert JM, Kontermann RE. The present and future of bispecific antibodies for cancer therapy. Nat Rev Drug Discov. 2024;23(4):301–19. https://doi.org/10.1038/s41573-024-00896-6

Li H, Saw PE, Song E. Challenges and strategies for next-generation bispecific antibody-based antitumor therapeutics. Cell Mol Immunol. 2020;17(5):451–61. https://doi.org/10.1038/s41423-020-0417-8

Lim SI. Fine-tuning bispecific therapeutics. Pharmacol Ther. 2020;212:107582. https://doi.org/10.1016/j.pharmthera.2020.107582

Liu S, Nguyen JB, Zhao Y, Schussler S, Kim S, Qiu H, et al. Development of a platform method for rapid detection and characterization of domain-specific post-translational modifications in bispecific antibodies. J Pharm Biomed Anal. 2024;244:116120. https://doi.org/10.1016/j.jpba.2024.116120

Liu Z, Leng EC, Gunasekaran K, Pentony M, Shen M, Howard M, et al. A novel antibody engineering strategy for making monovalent bispecific heterodimeric IgG antibodies by electrostatic steering mechanism. J Biol Chem. 2015;290(12):7535–62. https://doi.org/10.1074/jbc.m114.620260

Menon AP, Moreno B, Meraviglia-Crivelli D, Nonatelli F, Villanueva H, Barainka M, et al. Modulating T cell responses by targeting CD3. Cancer. 2023;15(4):1189. https://doi.org/10.3390/cancers15041189

Middelburg J, Kemper K, Engelberts P, Labrijn AF, Schuurman J, van Hall T. Overcoming challenges for CD3-bispecific antibody therapy in solid tumors. Cancer. 2021;13(2):287. https://doi.org/10.3390/cancers13020287

Middelburg J, Sluijter M, Schaap G, Göynük B, Lloyd K, Ovcinnikovs V, et al. T-cell stimulating vaccines empower CD3 bispecific antibody therapy in solid tumors. Nat Commun. 2024; 15(1):48. https://doi.org/10.1038/s41467-023-44308-6

National Biomedical Research Foundation. Atlas of protein sequence and structure. Silver Spring, MD: National Biomedical Research Foundation; 1978.

Niquille DL, Fitzgerald KM, Gera N. Biparatopic antibodies: therapeutic applications and prospects. MAbs. 2024;16(1):2310890. https://doi.org/10.1080/19420862.2024.2310890

Paul S, Konig MF, Pardoll DM, Bettegowda C, Papadopoulos N, Wright KM, et al. Cancer therapy with antibodies. Nat Rev Cancer. 2024;24(6):399–426. https://doi.org/10.1038/s41568-024-00690-x

Raina M, Moghal A, Kano A, Jerums M, Schnier PD, Luo S, et al. Reduced amino acid specificity of mammalian tyrosyl-tRNA synthetase is associated with elevated mistranslation of Tyr codons. J Biol Chem. 2014;289(25):17780–90. https://doi.org/10.1074/jbc.m114.564609

Saini S, Kumar Y. Chapter 9–Bispecific Antibodies: A Promising Entrant in Cancer Immunotherapy. In: Hasija Y., editor. Translational Biotechnology. Academic Press; Cambridge, MA, USA: 2021. pp. 233–66.

Smith EJ, Olson K, Haber LJ, Varghese B, Duramad P, Tustian AD, et al. A novel, native-format bispecific antibody triggering T-cell killing of B-cells is robustly active in mouse tumor models and cynomolgus monkeys. Sci Rep. 2015;5(1):17943. https://doi.org/10.1038/srep17943

Surowka M, Klein C. A pivotal decade for bispecific antibodies? MAbs. 2024;16(1):2321635. https://doi.org/10.1080/19420862.2024.2321635

Tustian AD, Endicott C, Adams B, Mattila J, Bak H. Development of purification processes for fully human bispecific antibodies based upon modification of protein a binding avidity. MAbs. 2016;8(4):828–38. https://doi.org/10.1080/19420862.2016.1160192

Wei B, Berning K, Quan C, Zhang YT. Glycation of antibodies: modification, methods and potential effects on biological functions. MAbs. 2017;9(4):586–94. https://doi.org/10.1080/19420862.2017.1300214

Wei J, Yang Y, Wang G, Liu M. Current landscape and future directions of bispecific antibodies in cancer immunotherapy. Front Immunol. 2022;13:1035276. https://doi.org/10.3389/fimmu.2022.1035276

Willems A, Schoonooghe S, Eeckhout D, Jaeger GD, Grooten J, Mertens N. CD3 × CD28 cross-interacting bispecific antibodies improve tumor cell dependent T-cell activation. Cancer Immunol Immunother. 2005;54(11):1059–71. https://doi.org/10.1007/s00262-005-0671-8

Williams WB, Meyerhoff RR, Edwards RJ, Li H, Manne K, Nicely NI, et al. Fab-dimerized glycan-reactive antibodies are a structural category of natural antibodies. Cell. 2021;184(11):2955–2972.e25. https://doi.org/10.1016/j.cell.2021.04.042

Xu X, O'Callaghan JA, Guarnero Z, Qiu H, Li N, Potocky T, et al. Low pK a of Lys promotes glycation at one complementarity-determining region of a bispecific antibody. Biophys J. 2022; 121(6):1081–93. https://doi.org/10.1016/j.bpj.2022.02.002

Zhang K, Liu X. Mixed-mode chromatography in pharmaceutical and biopharmaceutical applications. J Pharm Biomed Anal. 2016; 128:73–88. https://doi.org/10.1016/j.jpba.2016.05.007

Zhang L, Patapoff T, Farnan D, Zhang B. Improving pH gradient cation-exchange chromatography of monoclonal antibodies by controlling ionic strength. J Chromatogr A. 2013;1272:56–64.

SUPPORTING INFORMATION

Additional supporting information can be found online in the Supporting Information section at the end of this article.

How to cite this article: Nguyen JB, Liu S, Howie DA, Oberholtzer ZR, Ong ET, Rao R, et al. Comparison of enriched charge variants from different anti-CD3 bispecific antibodies reveals differential susceptibility of each bispecific arm to post-translational modification. Protein Science. 2025;34(4):e70079. https://doi.org/10.1002/pro.70079